Intermetallics 11 (2003) 995–1013
www.elsevier.com/locate/intermet

Thermodynamic properties of the Al–Nb–Ni system

Yong Du[a,b,*], Y.A. Chang[a], Weiping Gong[b], Baiyun Huang[b], Honghui Xu[b], Zhanpeng Jin[b], F. Zhang[c], S.-L. Chen[c]

[a]*Department of Materials Science and Engineering, University of Wisconsin-Madison, 1509 University Avenue, Madison, WI 53706-1595, USA*
[b]*State Key Laboratory of Powder Metallurgy, Central South University, Changsha, Hunan, 410083, PR China*
[c]*CompuTherm LLC, 437 S. Yellowstone Dr., Suite 217, Madison, WI 53706, USA*

Received 1 July 2002; accepted 30 May 2003

Abstract

This paper provides a consistent thermodynamic data set for the whole Al–Nb–Ni ternary system via thermodynamic modeling. The order/disorder transitions between disordered bcc_A2 and ordered bcc_B2 phases as well as between disordered fcc_A1 and ordered $L1_2$ phases are treated using a two-sublattice model. The calculations indicate that the disordered and ordered phases can be described with a single equation. All of the experimental phase diagram data available from the literature are critically reviewed and assessed using thermodynamic models for the Gibbs energies of individual phases. Inconsistent experimental information is identified and ruled out. Optimal thermodynamic parameters are then obtained by considering reliable literature data. Comprehensive comparisons between the calculated and measured phase diagrams show that almost all the accurate experimental information is satisfactorily accounted for by the present thermodynamic description.

Keywords: A. Ternary alloy systems; B. Phase diagram; B. Thermodynamic and thermochemical properties; B. Order/disorder transformations; E. Phase diagram prediction

1. Introduction

A thorough knowledge of the phase equilibria and thermodynamic properties of the superalloys is of fundamental importance in many applications, such as outer space and deep sea explorations [1], structural applications at elevated temperatures [2,3], and surface coating for high resistance to oxidation and corrosion [4]. In addition to the technological importance, the order/disorder transformations between disordered γ (fcc_A1) and ordered γ′($L1_2$–$AlNi_3$) phases, as well as between the disordered bcc_A2 and ordered bcc_B2, are of basic scientific interest.

The Al–Nb–Ni ternary system is extremely complex and involves 3 ternary compounds [5–9], T_1–$AlNbNi_2$ with Pearson symbol *cF16* and Space group *Fm3m*, T_2–$Nb(Al,Ni)_2$ with Pearson symbol *hP12* and Space group $P6_3/mmc$, and T_3–$Nb_6(Al,Ni)_7$ with Pearson symbol *oP52* and Space group *Pnam* [7]. Since the early work by Mints et al. [10], there have been extensive measurements of the phase equilibria in the Al–Nb–Ni system [7,8,11–25]. However, the data reported in these studies show noticeable discrepancies. Based on limited experimental data, Kaufman and Nesor [26] computed the Ni-rich corner of the Al–Nb–Ni ternary phase diagram. To the best of our knowledge, neither thermodynamic measurement nor thermodynamic modeling in the whole ternary system has been performed. The purposes of the present work are (I) to critically evaluate the experimental phase diagram data available for the Al–Nb–Ni system and (II) to obtain a self-consistent set of thermodynamic parameters for this system.

2. Evaluation of experimental data from the literature

To facilitate reading, the symbols denoting the phases in the Al–Nb–Ni system are listed in Table 1.

Using X-ray diffraction (XRD) and thermal analysis (TA), Mints et al. [10] constructed the pseudo-binary

* Corresponding author. Tel.: +86-731-8836213; fax: +86-731-8710855.
E-mail address: yong-du@mail.csu.edu.cn (Y. Du).

0966-9795/$ - see front matter © 2003 Elsevier Ltd. All rights reserved.
doi:10.1016/S0966-9795(03)00123-7

Table 1
List of the symbols to denote the phases in the Al-Nb-Ni system

Symbol	Phase
L	Liquid
(Al),(Nb),(Ni)	Solid solutions based on fcc Al, bcc Nb, fcc Ni, respectively
Al_3Ni	Binary Al_3Ni compound
Al_3Ni_2	Binary Al_3Ni_2 compound
Al_3Ni_5	Binary Al_3Ni_5 compound
B2	An ordered phase based on the bcc structure
bcc_A2	Disordered bcc phase
$L1_2$	An ordered phase based on fcc structure
fcc_A1	Disordered fcc phase
$NbNi_3$	Solid solution based on the $NbNi_3$ phase
NbNi	Solid solution based on the NbNi phase
Al_3Nb	Binary Al_3Nb compound
$AlNb_2$	Solid solution based on the $AlNb_2$ phase
$AlNb_3$	Binary $AlNb_3$ compound
T_1	Ternary compound $AlNbNi_2$
T_2	Ternary compound $Nb(Al,Ni)_2$
T_3	Ternary compound $Nb_6(Al,Ni)_7$

$AlNi_3$–$NbNi_3$ phase diagram in the temperature range 800–1400 °C. For this isopleth, only the pseudo-binary eutectic point of $L \Longleftrightarrow AlNi_3 + NbNi_3$ is employed in the modeling since it is generally believed that the measured eutectic temperature is more accurate than the measured liquidus. The approximate initial and final crystallization temperatures as well as the solubility of $NbNi_3$ in $AlNi_3$ were measured by Mints et al. [10]. These data are used to check the finally calculated $AlNi_3$–$NbNi_3$ phase diagram. More reliable solubility data between $NbNi_3$ and $AlNi_3$ are given by subsequent investigators [11,14,17,21–23]. By means of the XRD technique, Arbuzov and Chuprina [11] obtained six solubility data points for $NbNi_3$ in $AlNi_3$ in a narrow temperature range 1285–1305 °C. These data are also not utilized in the optimization but rather used for comparison with the calculated phase diagram. Using metallography and electron probe microanalysis (EPMA), Thompson and Lemkey [15] reinvestigated the eutectic composition of the pseudo-binary $AlNi_3$–$NbNi_3$ system and the mutual solubilities between $AlNi_3$ and $NbNi_3$ at 1280 °C. Within estimated experimental errors, the values published by Thompson and Lemkey [15] agree with those of Mints et al. [10]. The data from Thompson and Lemkey [15] are used to check the calculated $AlNi_3$–$NbNi_3$ isopleth. A ternary eutectic reaction, $L \Longleftrightarrow (Ni) + L1_2 + NbNi_3$, was determined to occur at 1270 °C by Lemkey and Thompson [18] using differential thermal analysis (DTA) and optical microscopy. This eutectic point is utilized in the modeling.

Based on TA, hardness measurement, XRD, and metallographic observations, Kornilov et al. [12] established that a pseudo-binary eutectic exists between B2 and T_2. The phase relationship data published by Kornilov et al. [12] are considered to be approximate because (i) the experimentally measured homogeneity range for T_2 [12] is much wider than that resulting from the subsequent work [7, 8] and (ii) the measured solubility of Nb in B2 [12] is much less than the expected value from the measurement on B2 in equilibrium with T_1 [20]. In spite of this, the pseudo-binary eutectic point and the congruent melting temperature of T_2 [12] are included in the optimization with a low weight factor, since these data are the only literature data in this region.

Based on 82 alloys, Benjamin et al. [7] determined the entire isothermal section at 1140 °C by means of XRD method and metallography. These authors [7] found three ternary phases, T_1, T_2, and T_3. A complete isothermal section at 900 °C was established by Markiv et al. [8] based on XRD examination for 150 alloys. The work of Benjamin et al. [7] and Markiv et al. [8] agrees well in the homogeneity ranges of T_1 and T_2, as well as with the phase equilibria associated with T_1, T_2, $NbNi_3$, Al_3Nb, and the various Al–Ni phases. Markiv et al. [8] did not observe the T_3 phase and found a small solubility (≈3 at.%) for Al in NbNi at 900 °C. Benjamin et al. [7] showed that NbNi is stable up to 30 at.% Al at 1140 °C. Using XRD, Hund and Raman [13] examined a portion of the isothermal section at 1000 °C and indicated that NbNi is stable with as much as 35 at.% Al. This result [13] is in good agreement with that of Benjamin et al. [7]. The existence of the T_3 phase was also confirmed by Hund and Raman [13]. However, Hund and Raman [13] reported that the T_3 phase has a smaller homogeneity range than that given by Benjamin et al. [7]. They [13] also found a ternary phase μ′ with higher Al content, the structure of which is similar to T_3. However, no supporting evidence for this change in structure could be found. If the results of the above three investigations [7,8,13] are correct, it is conceivable that (i) T_3 is a high-temperature phase stable above

Table 2
Optimized thermodynamic parameters in the Al–Nb–Ni system[a]

Liquid: Model (Al, Nb, Ni)$_1$

$^{ex}G^{L}_{Al,Nb,Ni} = x_{Al}\cdot x_{Nb}\cdot x_{Ni}\,(-\underline{140\,283}\times x_{Al} - \underline{107\,416}\times x_{Nb} - \underline{6\,811}\times x_{Ni})$

fcc_A1: Model (Al, Nb, Ni)$_1$

$^{ex}G^{fcc}_{Al,Nb,Ni} = x_{Al}\cdot x_{Nb}\cdot x_{Ni}\,(0\cdot x_{Al} + 0\cdot x_{Nb} + \underline{59\,427}\cdot x_{Ni})$

DisL1$_2$: Model (Al,Nb,Ni)$_1$

$^{o}L^{DisL1_2}_{Al,Nb} = {}^{o}L^{fcc}_{Al,Nb} + T,\ {}^{1}L^{DisL1_2}_{Al,Nb} = {}^{1}L^{fcc}_{Al,Nb},\ {}^{2}L^{DisL1_2}_{Al,Nb} = {}^{2}L^{fcc}_{Al,Nb}$

$^{o}L^{DisL1_2}_{Nb,Ni} = {}^{o}L^{fcc}_{Nb,Ni} + T,\ {}^{1}L^{DisL1_2}_{Nb,Ni} = {}^{1}L^{fcc}_{Nb,Ni}$

L1$_2$: Model (Al,Nb,Ni)$_{0.75}$(Al,Nb,Ni)$_{0.25}$

$U1_{AlNb} = \underline{8\,675}$

$U1_{NbNi} = \underline{-4\,047}$

$^{o}G^{L1_2}_{Al:Nb} = {}^{o}G^{L1_2}_{Nb:Al} = 3\times U1_{AlNb}$

$^{o}L^{L1_2}_{Al,Nb:Al} = {}^{o}L^{L1_2}_{Al,Nb:Nb} = {}^{o}L^{L1_2}_{Al,Nb:Ni} = 6\times U1_{AlNb}$

$^{o}G^{L1_2}_{Nb:Ni} = {}^{o}G^{L1_2}_{Ni:Nb} = 3\times U1_{NbNi}$

$^{o}L^{L1_2}_{Nb,Ni:Al} = {}^{o}L^{L1_2}_{Nb,Ni:Nb} = {}^{o}L^{L1_2}_{Nb,Ni:Ni} = 6\times U1_{NbNi}$

NbNi$_3$: Model (Nb, Ni)$_{0.75}$(Al, Nb, Ni)$_{0.25}$

$^{o}G^{NbNi_3}_{Nb:Al} - 0.75\ {}^{o}G^{bcc}_{Nb} - 0.25\ {}^{o}G^{fcc}_{Al} = -15\,000$[b]

$^{o}G^{NbNi_3}_{Ni:Al} - 0.75\ {}^{o}G^{fcc}_{Ni} - 0.25\ {}^{o}G^{fcc}_{Al} = -31\,615$[b]

NbNi: Model (Al, Nb, Ni)$_{7/13}$Nb$_{6/13}$

$^{o}G^{NbNi}_{Al:Nb} - (7/13)\ {}^{o}G^{fcc}_{Al} - (6/13)\ {}^{o}G^{bcc}_{Nb} = -19\,555$[b]

$L^{NbNi}_{Al,Ni:Nb} = \underline{-68\,172}$

B2: Model (Al, Nb, Ni)$_{0.5}$(Nb, Ni, Va)$_{0.5}$

$^{o}G^{B2}_{Al:Nb} - 0.5\ {}^{o}G^{bcc}_{Al} - 0.5\ {}^{o}G^{bcc}_{Nb} = -21\,000$[b]

$^{o}G^{B2}_{Nb:Nb} - {}^{o}G^{bcc}_{Nb} = 15\,000$[b]

$^{o}G^{B2}_{Nb:Ni} - 0.5\ {}^{o}G^{bcc}_{Nb} - 0.5\ {}^{o}G^{bcc}_{Ni} = {}^{o}G^{B2}_{Ni:Nb} - 0.5\ {}^{o}G^{bcc}_{Nb} - 0.5\ {}^{o}G^{bcc}_{Ni} = 23\,500$[c]

$^{o}G^{B2}_{Nb::Va} - 0.5\ {}^{o}G^{bcc}_{Nb} = 41\,000 - 0.5\ T^{+}$

$L^{B2}_{Al,Nb:Ni} = \underline{-96\,263}$

AlNb$_2$: Model (Al)$_{4/15}$(Nb)$_{2/15}$(Al,Nb,Ni)$_{9/15}$

$G^{AlNb_2}_{Al:Nb:Ni} - (4/15)\ {}^{o}G^{fcc}_{Al} - (2/15)\ {}^{o}G^{bcc}_{Nb} - (9/15)\ {}^{o}G^{fcc}_{Ni} = -45000$[b]

$L^{AlNb_2}_{Al:Nb:Nb,Ni} = \underline{-15\,165}$

T$_1$: Model Al$_{0.25}$Nb$_{0.25}$ Ni$_{0.5}$

$^{o}G^{T1}_{Al:Nb:Ni} - 0.25\ {}^{o}G^{fcc}_{Al} - 0.25\ {}^{o}G^{bcc}_{Nb} - 0.5\ {}^{o}G^{fcc}_{Ni} = \underline{-76\,189} + \underline{18.26679}\ T$

T$_2$: Model Nb$_{1/3}$(Al,Ni)$_{2/3}$

$^{o}G^{T2}_{Nb:Al} - (1/3)\ {}^{o}G^{bcc}_{Nb} - (2/3)\ {}^{o}G^{fcc}_{Al} = -11\,240$[b]

$^{o}G^{T2}_{Nb:Ni} - (1/3)\ {}^{o}G^{bcc}_{Nb} - (2/3)\ {}^{o}G^{fcc}_{Ni} = -25\,695$[b]

$^{o}L^{T2}_{Nb:Al,Ni} = -135\,447 + 18.35612\ T$

$^{1}L^{T2}_{Nb:Al,Ni} = \underline{18\,783} - \underline{28.62357}\ T$

T$_3$: Model Nb$_{6/13}$(Al,Ni)$_{7/13}$

$^{o}G^{T3}_{Nb:Ni} - (6/13)\ {}^{o}G^{bcc}_{Nb} - (7/13)\ {}^{o}G^{fcc}_{Al} = -16\,945$[b]

$^{o}G^{T3}_{Nb:Al} - (6/13)\ {}^{o}G^{bcc}_{Nb} - (7/13)\ {}^{o}G^{fcc}_{Ni} = -23\,570$[b]

$^{o}L^{T3}_{Nb:Al,Ni} = \underline{-68\,428} - \underline{2.27666}\ T$

[a] In J/(mol of atom); temperature (T) in Kelvin. The Gibbs energies for the pure elements are from the SGTE compilation [33]. The thermodynamic parameters in the Al–Ni, Al–Nb, and Nb–Ni systems are taken from [28], [29], and [30], respectively. The underlined parameters were optimized in the present work.

[b] Due to the lack of experimental information, the Gibbs energies for the fictitious compounds were simply given fixed values relative to the mechanical mixing of the pure elements. These values were assessed by checking their influences on the calculated phase equilibria as well as based on the enthalpies of formation at 25 °C in the binary systems.

[c] Calculated from the equation $^{o}G^{B2}_{Nb::Va} = {}^{o}G^{B2}_{Nb:Nb} + {}^{o}G^{B2}_{Al:Va} - {}^{o}G^{B2}_{Al:Nb}$.

900 °C and (ii) the solid solubility for Al in NbNi changes sharply between 900 and 1140 °C. In the present work, T$_3$ is modeled to be a high-temperature compound. In a preliminary optimization, all of the solubility data for Al in NbNi [7,8,13] are utilized. It was found that the thermodynamic modeling cannot describe all of the solubility data. Lacking further experimental data, the solubility data from both groups of authors [7,13] are adopted, since they are consistent with each other.

The tie-line data between (Ni) and L1$_2$ at 800, 1080 and 1200 °C were measured by Guseva et al. [14] using the XRD method. The experimental values at 800 °C were excluded from the modeling since the tie-line along the Al–Ni binary side derived from these values shows a noticeable discrepancy (=5 at.%) from the generally accepted Al–Ni phase diagram [27,28]. The tie-line values at both 1080 and 1200 °C are used in the present modeling but assigned a relatively low weight factor.

The solid state equilibria in the Ni-rich region of the Al–Nb–Ni system have been measured by several groups of authors [16,17,19,21] using both XRD and metallography. Nash et al. [20] used metallography, XRD and EPMA to determine the phase equilibria at 1200 °C. Following the same method, Ueyama et al. [24] measured one tie-line between L1$_2$ and NbNi$_3$ at 1200 °C. Using EPMA technique, Jia et al. [23] investigated the phase equilibria among (Ni), L1$_2$ and B2 from 800 to 1300 °C. Within the estimated experimental uncertainties, the experimental values from [17,21,23,24] are consistent with each other. As a consequence, these values [17,21,23,24] at temperatures above 800 °C are included in the present optimization. However, the phase equilibia at 750 °C [17] are excluded from the modeling for the same reason as the data of Guseva et al. [14] at 800 °C. The experimental values from Nash et al. [20] are not utilized in the optimization since the Ni content of T$_1$ phase measured by them is substantially more than that anticipated from both groups of authors [7,8]. This may partly result from the existence of a small amount of T$_1$ phase in one alloy [20], and therefore the accuracy of EPMA was consequently diminished. Another reason not to include the data of Nash et al. [20] is that the reported solubility of Al in L1$_2$ at the (Ni) + L1$_2$ + NbNi$_3$ tie triangle [20] is about 3 at.% higher than those from several investigations [14,16,17,22]. Within the estimated experimental errors, the L1$_2$–NbNi$_3$ tie line measured by Nash et al. [20] is consistent with that from Ueyama et al. [24]. This tie line is compared with the finally calculated isothermal section at 1200 °C. In a preliminary optimization procedure, all of the experimental data published by Nash et al. [20] are tested along with the other experimental data. It was found that the modeling gives rise to a worse agreement with the other experimental data. The phase equilibrium data at 600 °C [19] are also not used

Table 3
Optimized thermodynamic parameters in the Al–Nb–Ni system[a]

Liquid: Model (Al, Nb, Ni)$_1$
${}^{ex}G^{L}_{Al,Nb,Ni} = x_{Al}\cdot x_{Nb}\cdot x_{Ni}\,(\underline{43\ 913}\times x_{Al} - \underline{414\ 404}\cdot x_{Nb} + \underline{16\ 252}\cdot x_{Ni})$
fcc_A1: Model (Al, Nb, Ni)$_1$
${}^{ex}G^{fcc}_{Al,Nb,Ni} = x_{Al}\cdot x_{Nb}\cdot x_{Ni}\,(0\times x_{Al} + 0\times x_{Nb} + \underline{59\ 427}\times x_{Ni})$
L1$_2$: Model (Al,Nb,Ni)$_{0.75}$(Al,Nb,Ni)$_{0.25}$
$U1_{AlNb} = \underline{8\ 675}$
$U1_{NbNi} = -\underline{4\ 047}$
${}^{o}G^{L1_2}_{Al:Nb} = {}^{o}G^{L1_2}_{Nb:Al} = 3\times U1_{AlNb}$
${}^{o}L^{L1_2}_{Al,Nb:Al} = {}^{o}L^{L1_2}_{Al,Nb:Nb} = {}^{o}L^{L1_2}_{Al,Nb:Ni} = 6\times U1_{AlNb}$
${}^{o}G^{L1_2}_{Nb:Ni} = {}^{o}G^{L1_2}_{Ni:Nb} = 3\times U1_{NbNi}$
${}^{o}L^{L1_2}_{Nb,Ni:Al} = {}^{o}L^{L1_2}_{Nb,Ni:Nb} = {}^{o}L^{L1_2}_{Nb,Ni:Ni} = 6\times U1_{NbNi}$
bcc_A2: Model (Al, Nb, Ni,Va)$_1$
$L^{bcc}_{Nb,Va} = \underline{300\ 000}$
${}^{ex}G^{bcc}_{Al,Nb,Ni} = x_{Al}\cdot x_{Nb}\cdot x_{Ni}\,(-\underline{100\ 000}\cdot x_{Al} + 0\cdot x_{Nb} - \underline{100\ 000}\cdot x_{Ni})$
B2: Model (Al, Nb, Ni,Va)$_{0.5}$(Al,Nb, Ni, Va)$_{0.5}$
$\alpha_{Al,Va} = G^{B2}_{Al:Va} - G^{bcc}_{Al:Va} = 10000 - T$ [39]
$\lambda_{Al,Va} = 150\ 000$ [39]
$\alpha_{Ni,Va} = G^{B2}_{Ni:Va} - G^{bcc}_{Ni:Va} = 162\ 397 - 27.40575T$ [39]
$\lambda_{Ni,Va} = -64\ 024 + 26.49419T$ [39]
$\alpha_{Al,Ni} = G^{B2}_{Al:Ni} - G^{fcc}_{Al} - G^{fcc}_{Ni} = -152\ 397 + 26.40575T$ [39]
$\lambda_{Al,Ni} = -52441 + 11.30117T$ [39]
$G^{B2}_{i:i} = 0$ (i = Al, Nb, Ni, Va) [44]
$G^{B2}_{Al:Va} = G^{B2}_{Va:Al} = 0.5(\alpha_{Al,Va} - \lambda_{Al,Va})$ [44]
$G^{B2}_{Ni:Va} = G^{B2}_{Va:Ni} = 0.5(\alpha_{Ni,Va} - \lambda_{Ni,Va})$ [44]
$G^{B2}_{Nb:Va} = G^{B2}_{Va:Nb} = \underline{0}$
$G^{B2}_{Al:Ni} = G^{B2}_{Al:Ni} = 0.5(\alpha_{Al,Ni} - \lambda_{Al,Ni})$ [44]
$G^{B2}_{Ni:Nb} = G^{B2}_{Nb:Ni} = -\underline{5000}$
$G^{B2}_{Al:Nb} = G^{B2}_{Nb:Al} = -\underline{5000}$

[a] In J/(mol of atom); temperature (T) in Kelvin. The Gibbs energies for the pure elements are from the SGTE compilation [33]. The thermodynamic parameters in the Al–Ni, Al–Nb, and Nb–Ni systems are taken from [31], [29], and [30], respectively. The underlined parameters were optimized in the present work.

in the modeling since the established Al_3Ni_2 single-phase region [19] is significantly wider than the generally accepted one [27,28]. The results of Cisse and Davies [16] are quite different from those [17,21,23,24] and are not accepted here.

By means of DTA, Hong et al. [22] measured the (Ni) solvus in the temperature range of 827–1327 °C. Following the same technique, the same group [25] also obtained the liquidus and solidus in the Ni-rich portion of the ternary system. Since the thermodynamic parameters evaluated using the experimental data indicated in the proceeding section should predict phase equilibria over wide temperature and composition ranges, it is of considerable interest to compare the calculated phase equilibria with the experimental values, which are not utilized in the modeling. The experimental data from [22,25] are used for such a comparison.

3. Thermodynamic models

In the present modeling, the thermodynamic parameters in the Al–Ni, Al–Nb, and Nb–Ni systems are taken from [28,29], and [30], respectively. Replacing the Al–Ni description of [28] by [31] resulted in nearly identical calculated results. The models employed to describe the ternary phases are presented in Tables 2 and 3. In the following, the analytical expressions for the ternary phases are briefly presented.

3.1. Liquid, fcc_A1, and bcc_A2 phases

The Gibbs energy of the ternary liquid is described by Redlich–Kister polynomial [32]:

$$\begin{aligned}{}^{o}G^{L}_{m} = {} & x_{Al}\cdot {}^{o}G^{L}_{Al} + x_{Nb}\cdot {}^{o}G^{L}_{Nb} + x_{Ni}\cdot {}^{o}G^{L}_{Ni} \\ & + R\cdot T(x_{Al}\times ln x_{Al} + x_{Nb}\times ln x_{Nb} + x_{Ni}\times ln x_{Ni}) \\ & + x_{Al}\cdot x_{Nb}\cdot L^{L}_{Al,Nb} + x_{Al}\cdot x_{Ni}\cdot L^{L}_{Al,Ni} \\ & + x_{Nb}\cdot x_{Ni}\cdot L^{L}_{Nb,Ni} + x_{Al}\cdot x_{Nb}\cdot x_{Ni}\cdot L^{L}_{Al,Nb,Ni}\end{aligned} \quad (1)$$

in which R is the gas constant, and x_{Al}, x_{Nb}, and x_{Ni} are the mole fractions of Al, Nb, and Ni, respectively. The standard element reference (SER) state [33], i.e. the stable structure of the element at 25 °C and 1 bar, is used as the Gibbs energy reference state. The parameters denoted $L^{L}_{i,j}$ are the interaction parameters from the binary systems. $L^{L}_{Al,Nb,Ni}$ is a ternary parameter to be evaluated in the present work. This parameter is expressed as follows:

$$L^{L}_{Al,Nb,Ni} = x_{Al}\cdot L^{L}_{Al} + x_{Nb}\cdot L^{L}_{Nb} + x_{Ni}\cdot L^{L}_{Ni} \quad (2)$$

For the fcc_A1 and bcc_A2 phases, the Gibbs energy of each phase is described by splitting it into a non-magnetic contribution (${}^{o}G^{nmg}$) and a magnetic one

(ΔG^{mg}). ${}^{o}G^{nmg}$ is given by an equation similar to Eq. (1). ΔG^{mg} is described by the Hillert–Jarl–Inden model [34,35].

3.2. Ternary compounds and binary phases extending into the ternary system

The ternary compound T_3 is treated as a line compound $Nb_6(Al,Ni)_7$ in view of the crystal structure data [9] and the composition range of Al/Ni ratio where this single phase was observed [7]. Thus in accordance with the general formula for the sublattice model [36,37], its Gibbs energy per mole of formula can be expressed as:

$$\begin{aligned} {}^{o}G_m^{T_3} = & y'_{Al}\cdot {}^{o}G_{Nb:Al}^{T_3} + y'_{Ni}\cdot {}^{o}G_{Nb:Ni}^{T_3} \\ & + 7\cdot R\cdot T\left(y'_{Al}\ln y'_{Al} + y'_{Ni}\ln y'_{Ni}\right) \\ & + y'_{Al}\cdot y'_{Ni}\cdot {}^{o}L_{Nb:Al,Ni}^{T_3} \end{aligned} \tag{3}$$

in which y'_{Al} and y'_{Ni} are the site fractions of Al and Ni in the sub-lattice $(Al,Ni)_7$, respectively. The Gibbs energies of the fictitious compounds ${}^{o}G_{Nb:Al}^{T_3}$ and ${}^{o}G_{Nb:Ni}^{T_3}$ are expressed relative to the Gibbs energies of nonmagnetic fcc Al, fcc Ni and bcc Nb at the same temperature.

Both groups of authors [7,8] indicated some range of solubility for the homogeneity of T_1 phase. However, their data are insufficient to define the homogeneity range. Consequently, T_1 is modeled as a stoichiometric $AlNbNi_2$ phase. In view of the nearly constant Nb content and the large composition range of Al/Ni ratio where the single T_2 phase was found [7,8], this phase is described with the model $Nb(Al,Ni)_2$.

Because of the negligible solid solubilities for the third element [7,8,19], Al_3Ni, Al_3Ni_2, Al_3Nb, and $AlNb_3$ are treated as pure binary phases. There is no experimental information on the solubility of Nb in Al_3Ni_5. In the present work, it is assumed that Al_3Ni_5 shows a negligible solubility for Nb. The remaining binary compounds show extended solubilities for the third element [7,8,17,19–22,24]. In the binary systems, $NbNi_3$, NbNi, and $AlNb_2$ are described with the sublattice models $(Nb,\mathbf{Ni})_3(\mathbf{Nb},Ni)_1$, $(\mathbf{Nb},Ni)_7Nb_6$, and $Al_4Nb_2(Al,\mathbf{Nb})_9$, respectively, where boldface **Nb** and **Ni** represent the major species in the sub-lattices. In order to reduce the number of adjustable parameters in the optimization, it is assumed that the third element enters only into one of the sublattices. The Gibbs energies of T_1, T_2, $NbNi_3$, NbNi, and $AlNb_2$ phases are defined in a fashion analogous to Eq. (3).

3.3. Ordered $L1_2$ phase

The ordered $L1_2$ phase in the Al–Nb–Ni system is modeled with the sub-lattice model $(Al,Nb,\mathbf{Ni})_{0.75}(\mathbf{Al},Nb,Ni)_{0.25}$. This model is a normal extension of the model used for the Al–Ni binary system by adding Nb to both sublattices. The ternary $L1_2$ phase has a contribution from the disordered ternary fcc_A1 phase, which is described by the model (Al,Nb,Ni). Ansara et al. [38,39] have derived an equation which allows the thermodynamic properties of the disordered phase to be evaluated independently. This is done by resolving the Gibbs energy into three terms:

$$\begin{aligned} G_m^{fcc\_Al,L1_2} = & G_m^{fcc\_A1}(x_{Nb}, x_{Ni}) \\ & + G_m^{L1_2}\left(y'_{Nb}, y'_{Ni}, y''_{Nb}, y''_{Ni}\right) \\ & - G_m^{L1_2}(x_{Nb}, x_{Ni}) \end{aligned} \tag{4}$$

where $y'_{Nb}$and y'_{Ni} are the site fractions of Nb and Ni in the first sublattice, and y''_{Nb}andy''_{Ni} in the second one. $G_m^{fcc\_A1}(x_{Nb}, x_{Ni})$ is the Gibbs energy of the disordered fcc_A1 phase. The second term, $G_m^{L1_2}(y'_{Nb},y'_{Ni},y''_{Nb},y''_{Ni})$, is described by the sub-lattice model and implicitly contains a contribution from the disordered state. The last term, $G_m^{L1_2}(x_{Nb}, x_{Ni})$, represents that contribution from the disordered state to the ordered one. When the site fractions are equal, *i.e.* $y'_{Nb}=y''_{Nb}$ and $y'_{Ni}=y''_{Ni}$, the last two terms cancel each other. In this case, Eq. (4) corresponds to the disordeded state. The reader is referred to [39,40] for more details about the model. Eq. (4) is implemented in the Pandat [41] and Thermo-Calc [42] software.

By replacing fcc_A1 with a new disordered phase ($DisL1_2$) in Eq. (4), Huang and Chang modeled the Al–Ni [27,28] and Al–Cr–Ni [40] systems. The parameters for $DisL1_2$ phase evaluated by Huang and Chang [27,28,40] are slightly different from those of really disordered fcc_A1 phase. Using a single Gibbs energy function for both $L1_2$ and fcc_A1, Ansara and Dupin [31,39] have also modeled the above two systems. In the present work, both approaches are tested separately in thermodynamic modeling.

3.4. Ordered B2 phase

The ordered ternary B2 phase is modeled as $(Al,Nb,Ni,Va)_{0.5}(Al,Nb,Ni,Va)_{0.5}$, where Va is a vacancy. In order to represent the Gibbs energies of both ordered B2 and disordered bcc_A2 phases using a single function, the ternary bcc_A2 is described by a model (Al,Nb,Ni,Va). Similar to the equation used to describe the thermodynamic behavior of $L1_2$ and fcc_A1, the Gibbs energy of both B2 and bcc_A2 is given by an equation of the form:

$$\begin{aligned} G_m^{bcc\_A2,B2} = & G_m^{bcc\_A2}(x_{Al}, x_{Nb}, x_{Ni}) \\ & + G_m^{B2}\left(y'_{Al}, y'_{Nb}, y'_{Ni}, y''_{Al}, y''_{Nb} y''_{Ni}\right) \\ & - G_m^{B2}(x_{Al}, x_{Nb}, x_{Ni}) \end{aligned} \tag{5}$$

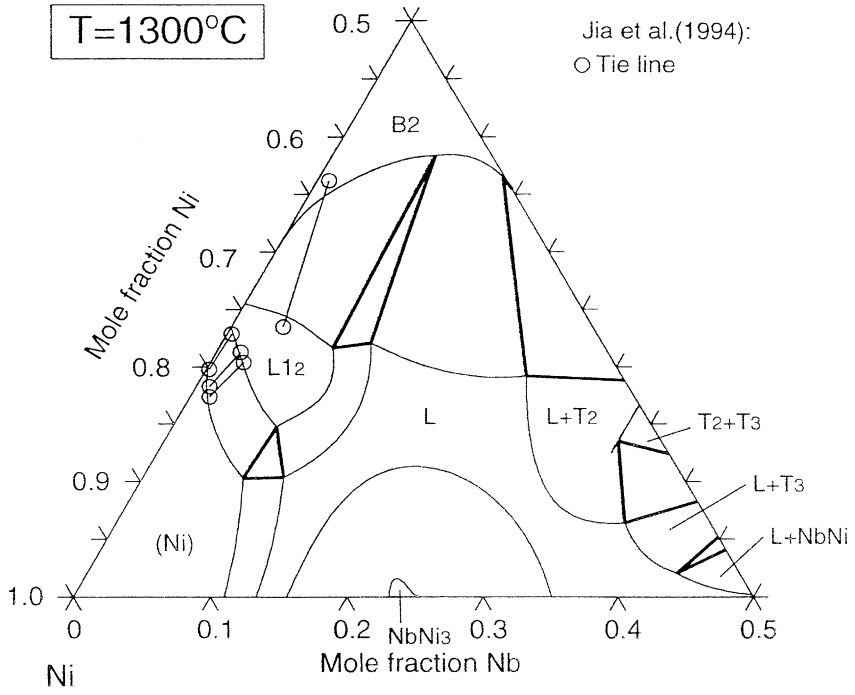

Fig. 1. Calculated 1300 °C isothermal section with the experimental data of Jia et al. [23]. For the abbreviations of the phases, see Table 1.

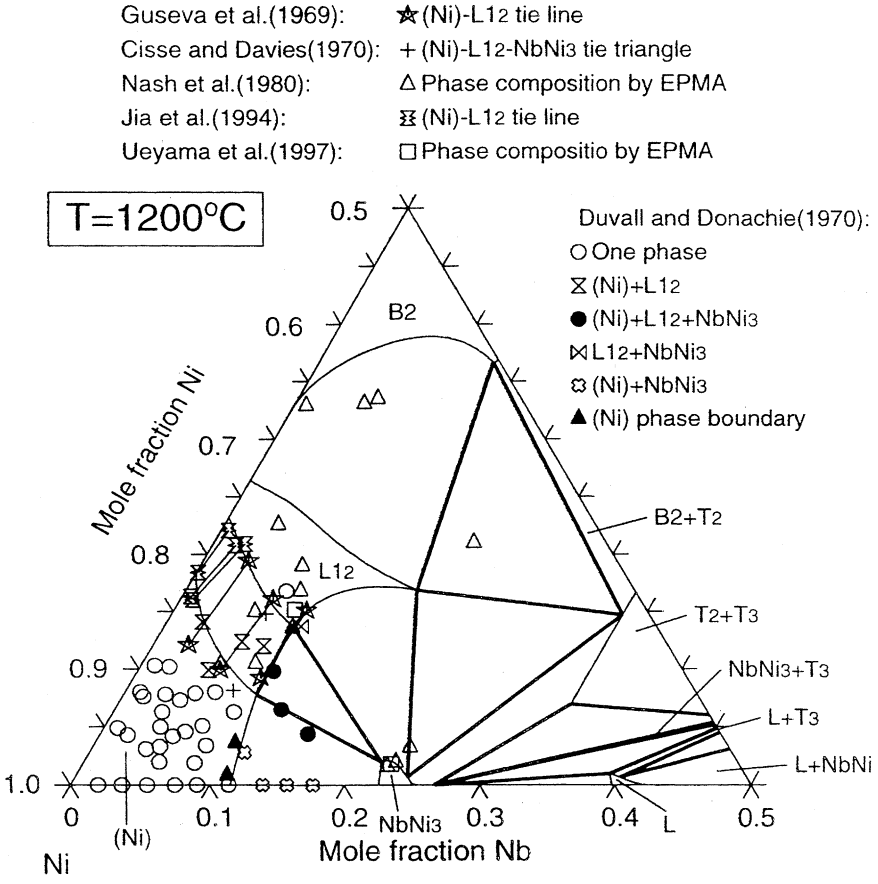

Fig. 2. Calculated 1200 °C isothermal section, compared with the experimental values from the literature [14,16,17,20,23,24]. For the abbreviations of the phases, see Table 1.

Equation (5) is compatible with descriptions of other B2 phases with anti-structure defects, such as the B2 phase in the Al-Fe system [43]. The B2 phase in the Al-Fe system is described by the model $(Al,Fe)_{0.5}(Al,Fe)_{0.5}$ [43]. The reader is referred to [31,44] for more details about Eq. (5).

By using a model $(Al,Cr,Ni)_{0.5}(Cr,Ni,Va)_{0.5}$ to describe the B2 phase, Huang and Chang [40] have assessed the ternary Al–Cr–Ni system. This model is also tested in the present modeling of the Al–Nb–Ni system.

4. Results and discussion

All of the calculations were performed with the Pandat program [41]. The model parameters were evaluated

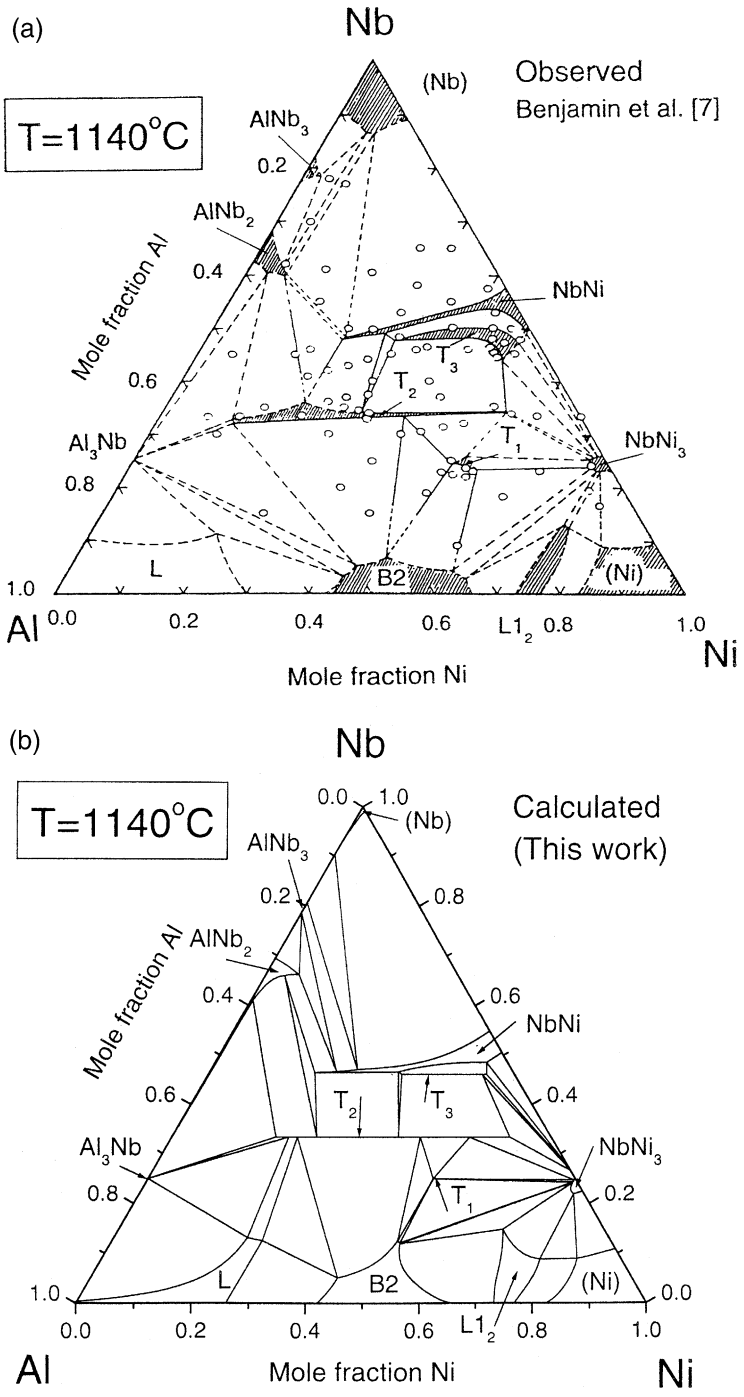

Fig. 3. Observed and calculated isothermal sections at 1140 °C: (a) observed section by Benjamin et al. [7]; (b) calculated section according to the present modeling. For the abbreviations of the phases, see Table 1.

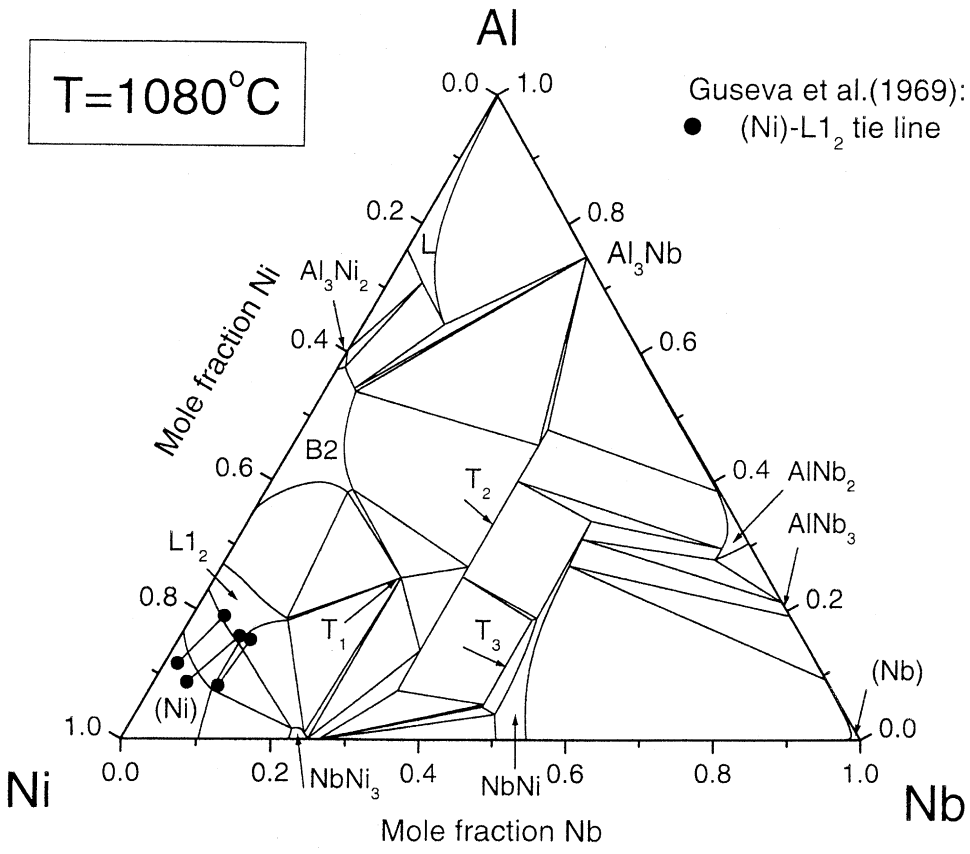

Fig. 4. Calculated 1080 °C isothermal section with the experimental data from Guseva et al. [14]. For the abbreviations of the phases, see Table 1.

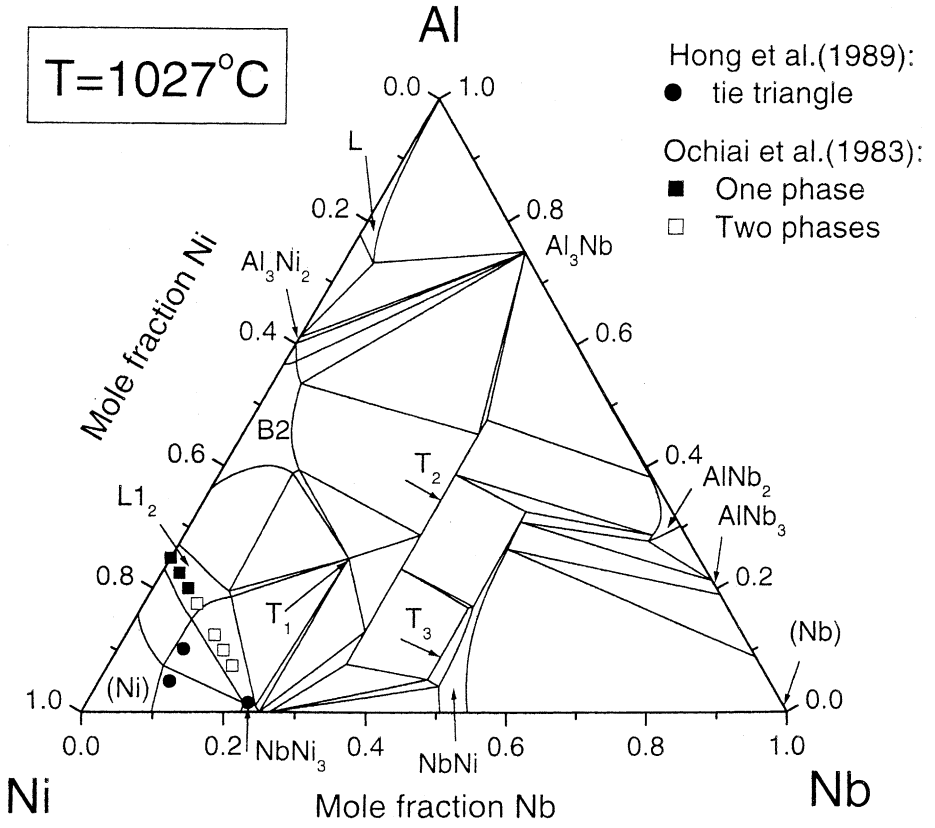

Fig. 5. Calculated 1027 °C isothermal section with the experimental data [21,22]. For the abbreviations of the phases, see Table 1.

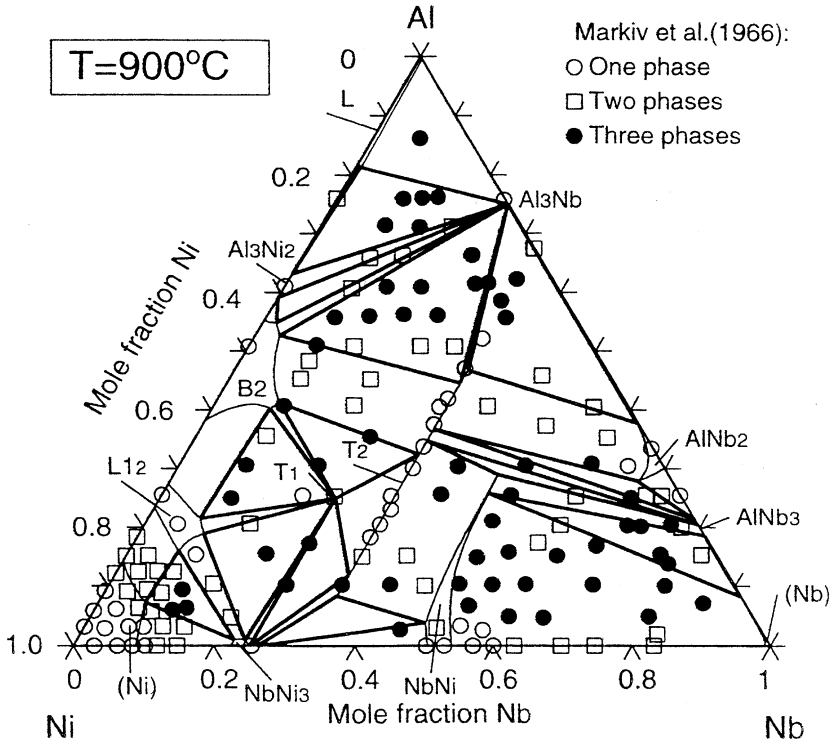

Fig. 6. Calculated 900 °C isothermal section, compared with the experimental data from Markiv et al. [8]. For the abbreviations of the phases, see Table 1.

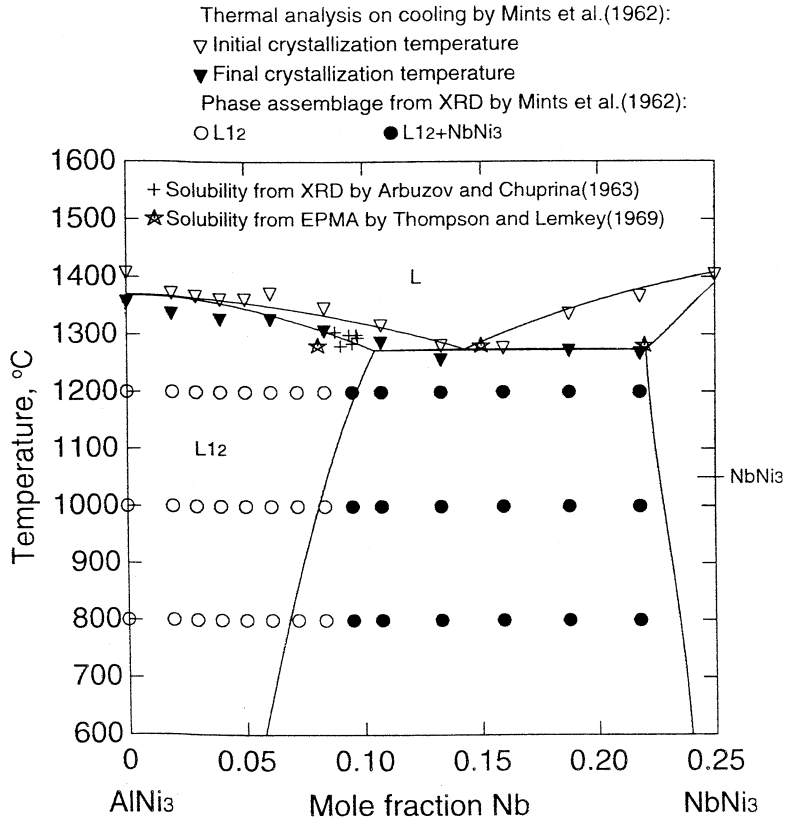

Fig. 7. Calculated isopleth from $AlNi_3$ to $NbNi_3$, compared with the experimental data [10,11,15]. For this isopleth, only the quasi-binary eutectic point of $L \Longleftrightarrow L1_2 + NbNi_3$ is used in the present modeling. For the abbreviations of the phases, see Table 1.

Table 4
Comparison between calculated and measured reaction temperatures and liquid compositions for some invariant equilibria in the Al-Nb-Ni system[a]

Source	Composition (at.% Al, at.% Ni)	Temperature (°C)
	$L \Longleftrightarrow T_2$	
Measured [12]	~33.3, ~33.3	~1597
Calculated (this work)[b]	41.8, 25	1588
Calculated (this work)[c]	43.2, 23.4	1615
	$L \Longleftrightarrow B2 + T_2$	
Measured [12]	~41.8, ~41.8,	~1437
Calculated (this work)[b]	38.6,38.6	1458
Calculated (this work)[c]	39.8, 39.8	1415
	$L \Longleftrightarrow L1_2 + NbNi_3$	
Measured [10]	9.3, 75	1280±10
Calculated (this work)[b]	10.5, 75	1276
Calculated (this work)[c]	9, 75	1284
	$L \Longleftrightarrow (Ni) + L1_2 + NbNi_3$	
Measured [18]	7.3, 79	1270±10
Calculated (this work)[b]	7.9, 78.6	1267
Calculated (this work)[c]	6.8, 78.5	1277

[a] For the abbreviations of the phases, see Table 1.
[b] The thermodynamic parameters shown in Table 2 are used in the calculation. In the modeling, the disordered fcc_A1 and ordered $L1_2$ phases are treated as separated phases. This is also the case for the disordered bcc_A2 and ordered B2 phases.
[c] The thermodynamic parameters listed in Table 3 are used in the calculation. In the modeling, the disordered fcc_A1 and ordered $L1_2$ phases are described using a single sub-lattice formalism. This is also the case for the disordered bcc_A2 and ordered B2 phases.

using the computer-operated optimization program PARROT [42], which works by minimizing the square sum of the differences between measured and calculated values. The step-by-step optimization procedure carefully described by Du et al. [45] was utilized in the present assessment. In the following paragraph, the strategy to evaluate thermodynamic parameters associated with the models after Hunag and Chang [28,40] is briefly described.

The parameters for liquid, fcc_A1, $L1_2$, Dis$L1_2$ (disordered part of $L1_2$), B2, $NbNi_3$, NbNi, $AlNb_2$, T_1, T_2, and T_3 are adjusted by using the experimental data selected in Section 2.

For liquid, it is possible to optimize the regular parameters L^L_{Al}, L^L_{Nb}, and L^L_{Ni} in Eq. (2) since the whole liquidus line along the isopleth $AlNi_3$–$NbNi_3$ [10] and the partial liquidus along the AlNi–Nb isopleth [12] are established. In the case of fcc_A1, only the regular parameter L^{fcc}_{Ni}, which makes a major contribution to the excess Gibbs energy of this phase in the Ni-rich side, can be adjusted because experimental data are only available in the Ni-rich side. According to the model of Huang and Chang [40], there is a metastable $L1_2$ phase in both the Al–Nb and Nb–Ni systems, with parameters $L^{DISL1_2}_{Al,Nb}$ and $U1_{AlNb}$, and $L^{DISL1_2}_{Nb,Ni}$ and $U1_{NbNi}$, respectively. The two binary order-independent parameters, $L^{DISL1_2}_{Al,Nb}$ and $L^{DISL1_2}_{Nb,Ni}$, were given values slightly above those of the corresponding binary fcc_A1 phases in order to make Dis$L1_2$ phase metastable throughout the entire temperature and composition ranges. Only two order-dependent parameters, $U1_{AlNb}$ and $U1_{NbNi}$, are optimized for the description of the ternary $L1_2$ phase. For the B2 phase, only the dominant ternary parameter $L^{B2}_{Al,Nb:Ni}$ is optimized and its value is taken to be constant. A constant regular parameter was introduced for both NbNi and $AlNb_2$. In the case of $NbNi_3$, the limited solubility data for Al can be well described without introducing any ternary parameter. For T_1 and T_3, a temperature-dependent regular parameter ($A + BT$) was introduced for each of them. In the case of T_2, a subregular model was found to be necessary because of its large homogeneity range in the ternary system. The assessed thermodynamic parameters corresponding to the model of Huang and Chang [28,40] are shown in Table 2. By using the parameters listed in this table, typical phase diagrams are calculated and compared with the experimental data.

In Fig. 1, the calculated isothermal section at 1300 °C is compared with the experimental values from Jia et al. [23]. The fit to the experimental data is excellent. Fig. 2 shows the calculated isothermal section at 1200 °C along with the experimental data [14,16,17,20,23,24]. Except for the data from Nash et al. [20], the other experimental values are well reproduced by the calculation within the estimated experimental errors. As shown in Fig. 1, the measured $L1_2$-B2 tie line at 1300 °C [23] is well reproduced by the present modeling. At relatively low temperature, such as 1200 °C, the $L1_2$-B2 tie line not far from the Al–Ni binary side should be close to that at 1300 °C. However, the measured $L1_2$-B2 tie line at 1200 °C [20] is quite different from that at 1300 °C

[23]. The experimentally measured $L1_2$-B2 tie line at 1300 °C and (Ni)-$L1_2$ tie line at both 1200 and 1300 °C [23] can be well described by the present calculation. This gives another gauge that the data published by Nash et al. [20] could be questionable.

In Fig. 3, the calculated isothermal section at 1140 °C is compared with the observed one [7]. In order to be in agreement with the original paper [7], this calculated isothermal section is shown with a different orientation from the other diagrams. The modeling can account for most of the phase assemblage data. Some discrepancies exist in the Nb-rich part. This could be attributed to the short annealing time (20 h at 1140 °C) used by Benjamin et al. [7]. True equilibrium could not be attained with

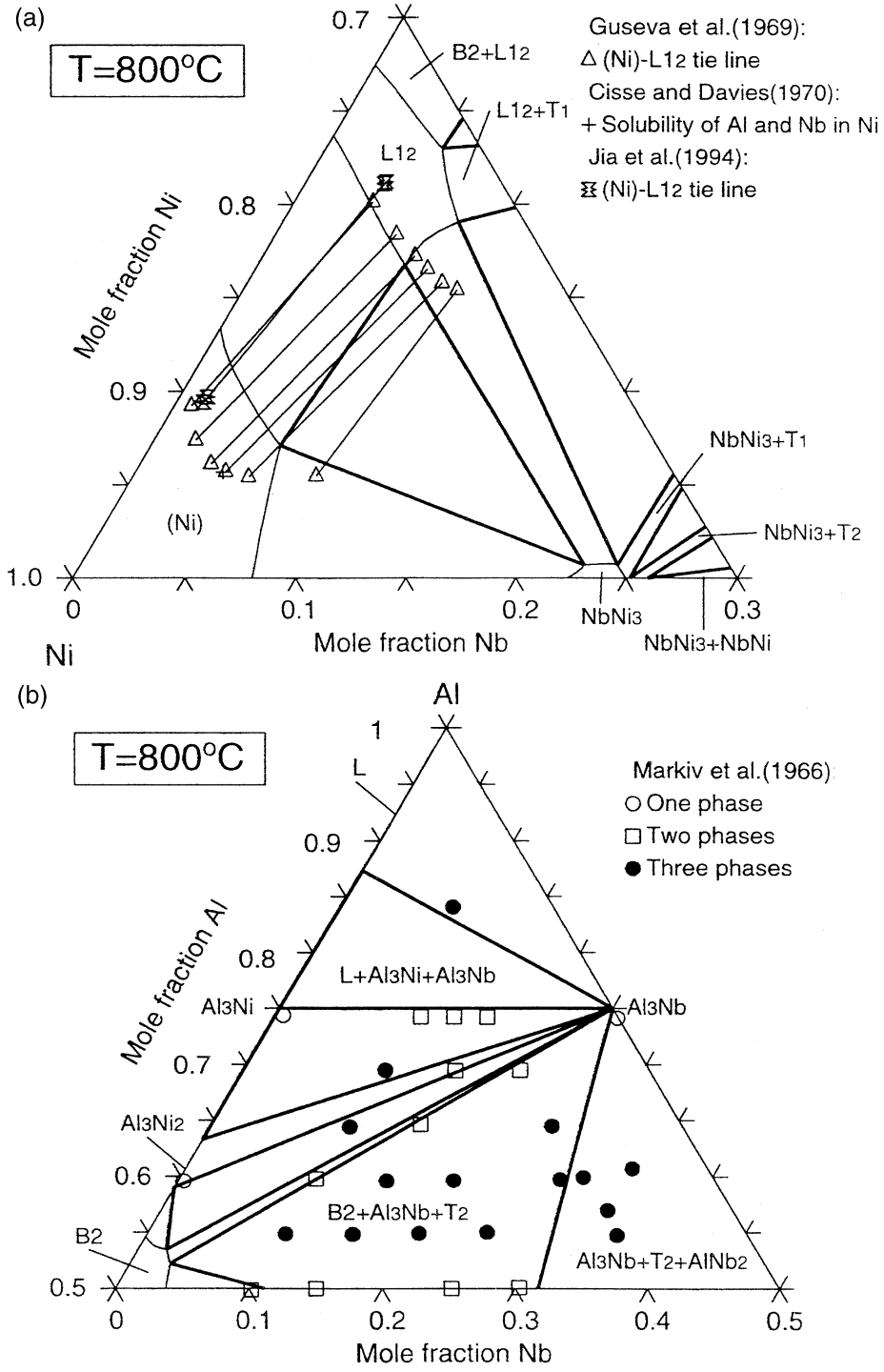

Fig. 8. Calculated 800 °C isothermal section, compared with the experimental data [8,14,16,23] which are not used in the optimization: (a) in the composition range of 70 at.% Ni to pure Ni; (b) in the composition range of 50 at.% Al to pure Al. For the abbreviations of the phases, see Table 1.

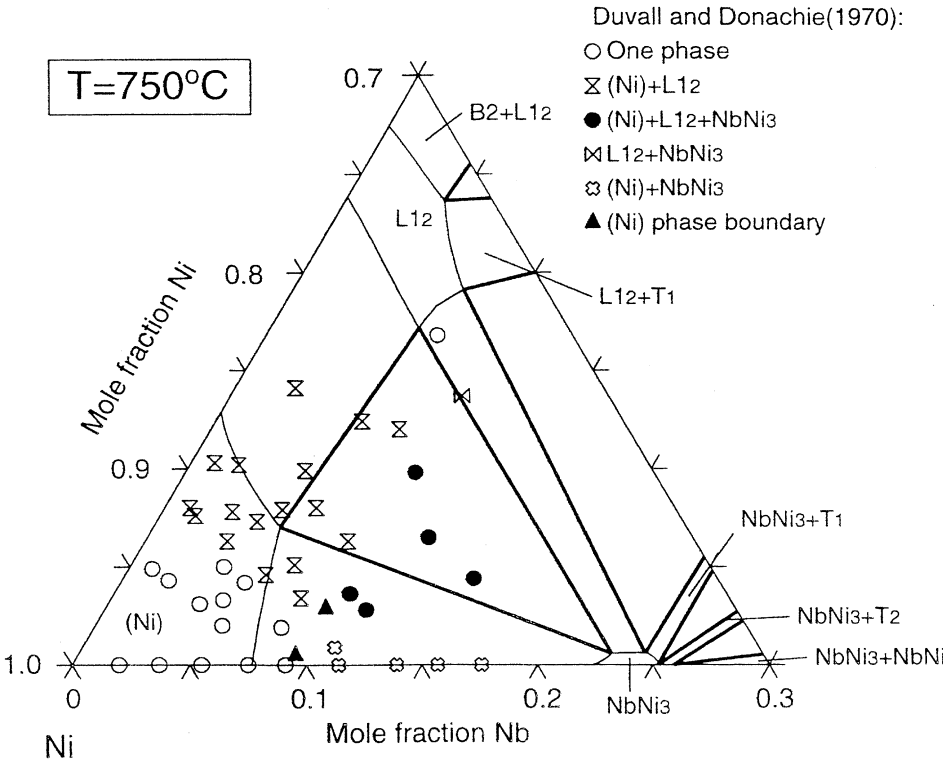

Fig. 9. Calculated 750 °C isothermal section, compared with the experimental values from Duvall and Donachie [17]. These experimental data are not utilized in the present modeling. For the abbreviations of the phases, see Table 1.

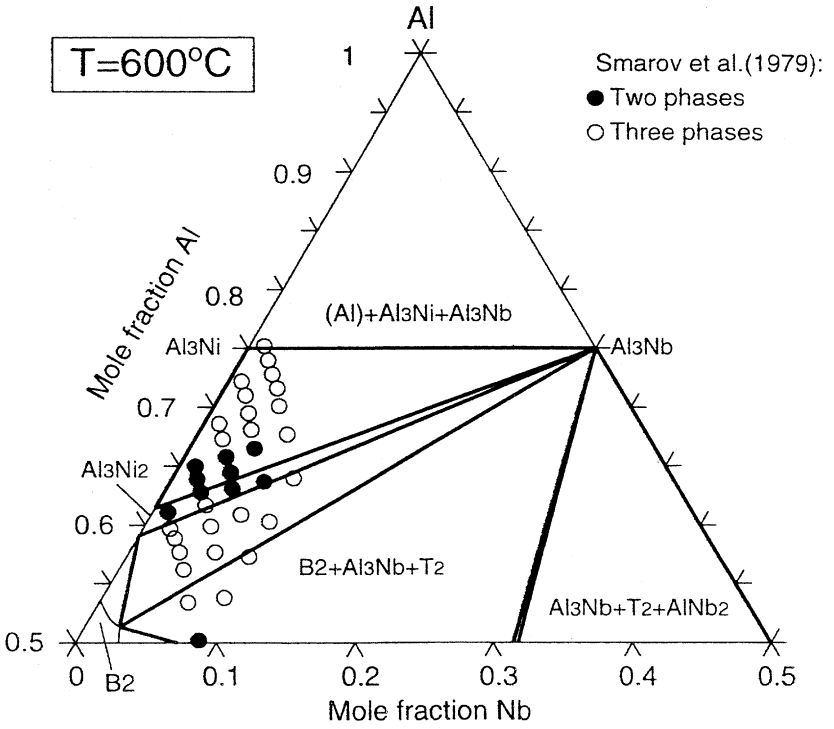

Fig. 10. Calculated 600 °C isothermal section, compared with the experimental data from Smarov et al. [19]. These experimental values are not used in the present modeling. For the abbreviations of the phases, see Table 1.

such short annealing in the Nb-rich portion. Fig. 4 presents the calculated isothermal section at 1080 °C with a few tie-line data from Guseva et al. [14], showing a reasonable agreement. In Fig. 5, the calculated isothermal section at 1027 °C is compared with the experimental values [21,22]. Except for one data point associated with $L1_2$, the other values are satisfactorily accounted for by the calculation.

Fig. 6 shows the calculated isothermal section at 900 °C along with the experimental values of Markiv et al. [8]. The phase assemblage data associated with T_1, T_2, $NbNi_3$, $AlNb_3$, and the various Al–Ni phases are

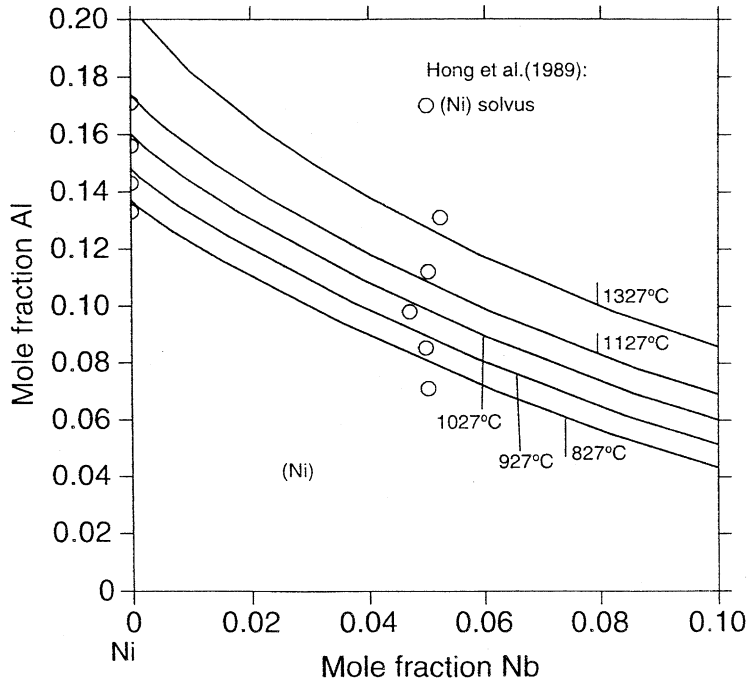

Fig. 11. Calculated (Ni) solvus, compared with the experimental data of Hong et al. [22]. Their experimental values are not used in the present modeling.

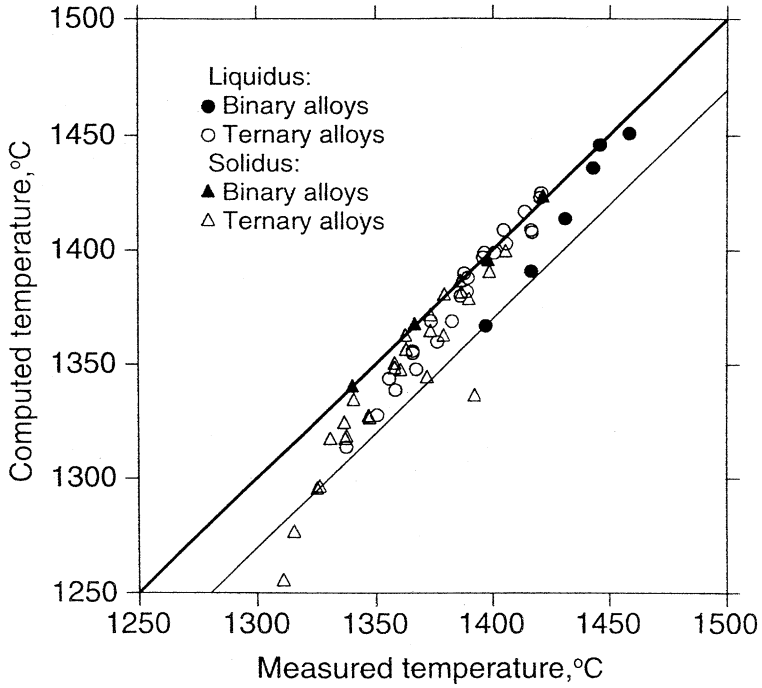

Fig. 12. Calculated liquidus and solidus in Ni-rich side of the Al-Nb-Ni system, compared with the experimental data from Miura et al. [25]. The experimental data from Miura et al. are not used in the present modeling. The light solid line corresponds to the maximum experimental uncertainty resulting from the measurements in the binary Al-Ni system. Along the thick diagonal line, the computed temperature is equal to the measured one.

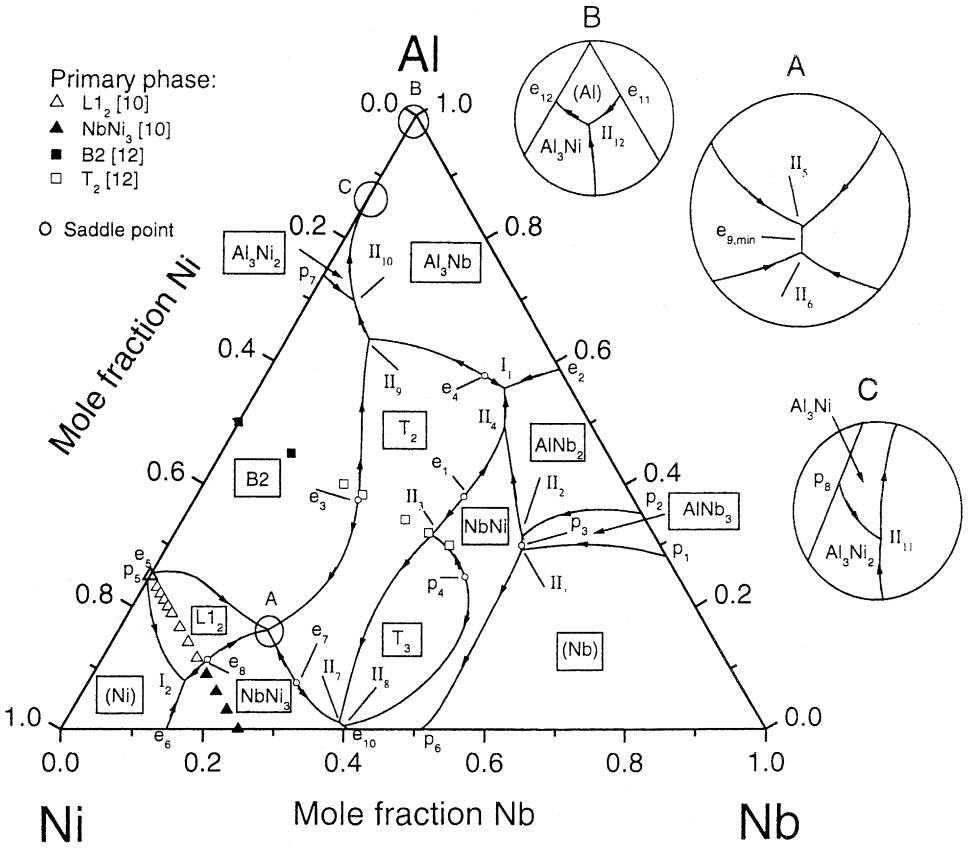

Fig. 13. Calculated liquidus projection in the Al-Nb-Ni system according to the present calculation. The measured [10,12] primary phase fields for $L1_2$, $NbNi_3$, B2, and T_2 are shown for a comparison with the calculation. For the abbreviations of the phases, see Table 1.

reasonably reproduced by the calculation within the estimated experimental errors. However, the phase assemblage data including the NbNi phase disagree with the computed ones. These discrepancies originate from the small solubility of Al in NbNi reported by Markiv et al. [8]. Both Benjamin et al. [7] and Hund and Raman [13] found that NbNi dissolve large amounts of Al.

The measured isopleth $AlNi_3$–$NbNi_3$ [10,11,15] is compared with the one calculated in Fig. 7. For this isopleth, only the pseudo-binary eutectic point is included in the optimization. In spite of this, the other experimental data are reasonably reproduced in view of the experimental uncertainties. The calculated solubility of Nb in $L1_2$ at 800 °C is lower than the experimental one [10] by 2 at.%.

Table 4 compares some of the calculated invariant reaction temperatures with the experimental observations [10,12,18]. Agreement is obtained within 10 K for three of the four established invariant reaction temperatures. No attempt was made to improve the fitting to the reaction $L \Longleftrightarrow B2 + T_2$ [12]. It has been pointed out that the data of Kornilov et al. [12] are only approximate since their work show some discrepancy with the bulk of the published work [7,8,20].

The calculated isothermal sections at 800, 750, and 600 °C are compared with the corresponding experimental data [8,14,16,17,19,23] in Figs. 8–10, respectively. These experimental data are not used in the parameter evaluation. As can be seen from Figs. 8(b) and 10, most of the experimental values [8,19] in Al-rich side are well reproduced by the modeling. A few phase assemblage data in the Al_3Ni_2–Al_3Nb two phase region [19] cannot be described by the calculation since the measured Al_3Ni_2 single [19] phase region along the Al–Ni binary system is much wider than the calculated one [28]. In the case of the Ni-rich side, as shown in Figs. 8(a) and 9, some discrepancies exist between the experimentally determined and calculated boundaries of the (Ni) phase. Again, these deviations result from the differences between the calculated and measured boundaries of (Ni) in the binary Al–Ni and Nb–Ni systems.

In this paragraph, we compare the Ni-rich solidus and liquidus predicted by using the thermodynamic parameters with two pieces of experimental information, which are not used in the modeling. Fig. 11 compares the predicted (Ni) solvus with the experimental data [22], showing an excellent agreement. A comparison of the model-predicted Ni-rich solidus and liquidus with

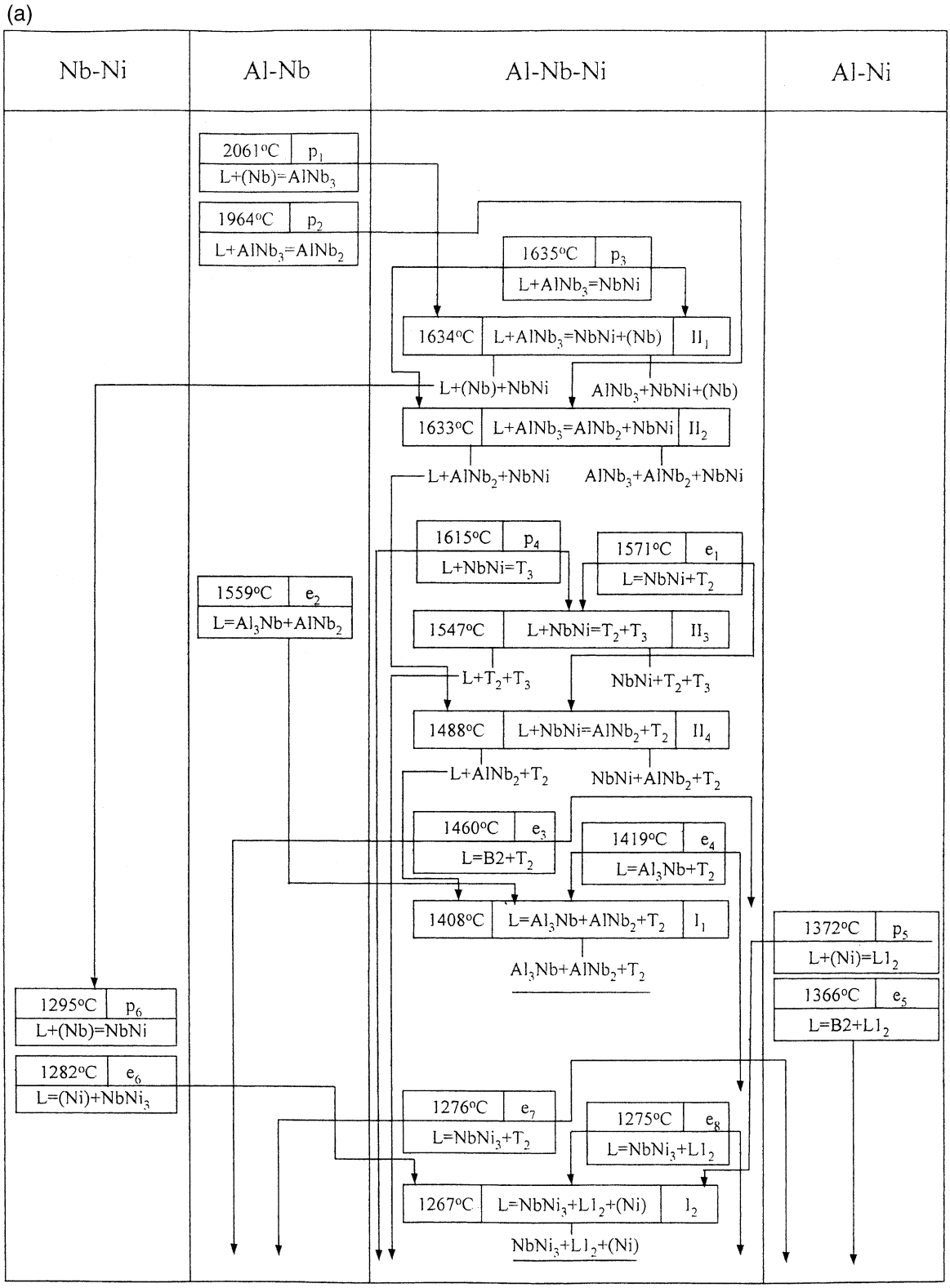

Fig. 14. The reaction scheme for the entire Al-Nb-Ni system according to the present calculation: (a) above 1267 °C; (b) between 1267 ° and 646 °C; and (c) solid state reactions. For the abbreviations of the phases, see Table 1.

(b)

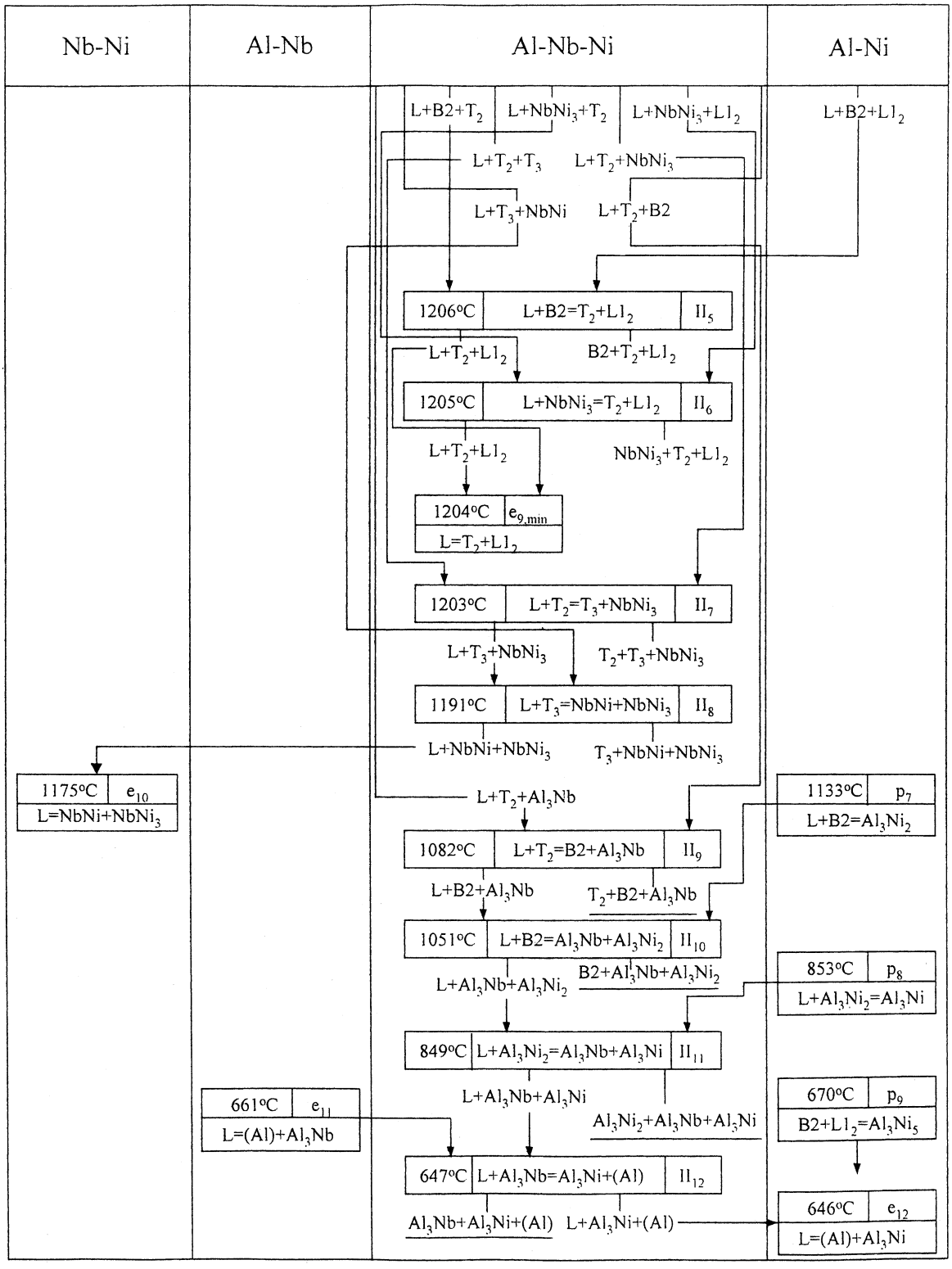

Fig. 14. *(continued)*

(c)

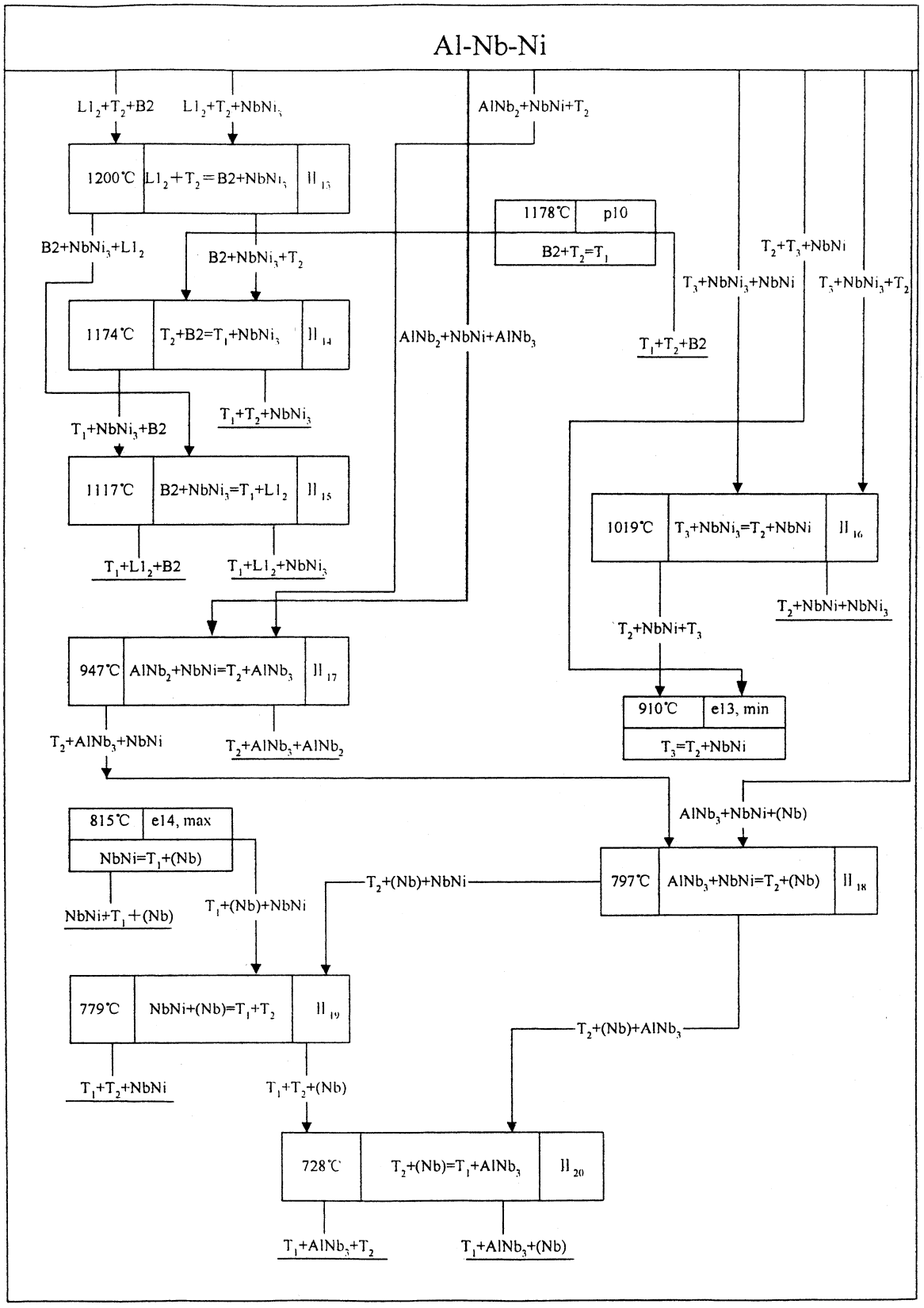

Fig. 14. *(continued)*

the experimental data [25] is made in Fig. 12 and also shows a good agreement. As shown in this figure, only three data points are outside the maximum experimental uncertainty resulting from the measurements in the binary Al–Ni system.

Finally, the calculated primary phases are shown in Fig. 13 along with the limited experimental data [10,12]. With the exception of two data points on T_2 [12], the other experimental values are well accounted for by the modeling. Better fitting to the two data points results in worse agreement with the other phase diagram data.

Fig. 14 gives the reaction scheme of the Al–Nb–Ni system. According to the present calculation, the T_2 compound has a congruent melting point of 1588 °C, which agrees reasonably with the experimental one 1597 °C [12]. Based on very limited experimental data, Kornilov et al. [12] suggested that the T_3 compound is probably formed by a peritectic reaction. The present modeling shows that T_3 is formed by the peritectic reaction $L + NbNi \Longleftrightarrow T_3$ at 1615 °C. The present calculation indicates that T_1 is formed by the solid state reaction $B2 + T_2 \Longleftrightarrow T_1$ at 1178 °C. Based on EPMA measurement on one alloy containing a small amount of T_1 phase, Nash et al. [20] suggested the existence of this ternary phase at 1200 °C. However, the Ni content of T_1 phase measured by Nash et al. [20] is substantially more than that anticipated from both groups of authors [7,8], who used more samples to determine the composition of T_1 phase at 1140 and 900 °C, respectively. Two of the eight saddle points, e_3 and e_8, are established by means of experiments [10,12]. Further experimental work is necessary to confirm the existence of the other saddle points and to investigate the melting behavior of both T_1 and T_3 phases more accurately.

The model of Ansara and Dupin [31,39,44], by which the Gibbs energy of both ordered and disordered phases is represented with a single equation, is also tested in the present work. By fixing the parameters of the other phases listed in Table 2, the parameters for liquid, fcc_A1, $L1_2$, bcc_A2, and B2 are reassessed. It was found that the calculated phase diagrams nearly coincide when the thermodynamic parameters of fcc_A1 and $L1_2$ associated with Huang and Chang's model is directly used in Ansara and Dupin's model. This is expected since the Gibbs energy of the $DisL1_2$ phase, which is taken to be the disordered part of $L1_2$ by Hunag and Chang, is very close to that of the fcc_A1 phase, which is the disordered part of $L1_2$ in Ansara and Dupin's model. The disordered bcc_A2 and ordered B2 phases are also modeled with a single equation in Ansara and Dupin's model. The binary ordering parameters, $G^T_{Cr:Si}$ and $G^T_{Cr:Si}$, and the ternary interaction parameter of the disordered bcc_A2 phase were adjusted in the present work. Assuming that no ordering occurs between the vacancies and Nb leads to $G^{B2}_{Nb:Va} = 0$. In addition, the symmetry of the model for B2 phase has been taken into account by imposing the following equation $G^{B2}_{i:j} = G^{B2}_{j:i}$ (i, j = Al, Nb, Ni, Va). The evaluated thermodynamic parameters corresponding to the model of Ansara and Dupin [31,39,44] are listed in Table 3. In general, the phase equilibria calculated from both models are identical within estimated experimental errors, as shown in Table 4. To conserve space, no diagrams are presented to show comparisons with the other experimental data for Ansara and Dupin's model.

5. Summary

(i) Phase equilibrium data of the Al–Nb–Ni system reported in the literature are critically reviewed. On the basis of reliable experimental data, a thermodynamic description for the whole ternary system is developed by means of thermodynamic modeling. Comprehensive comparisons show that most of the experimental data are well accounted for by the present description.

(ii) The ordered ternary B2 phase is described with a symmetric model $(Al,Nb,Ni,Va)_{0.5}$ $(Al,Nb,Ni,Va)_{0.5}$ and an asymmetric one $(Al,Nb,Ni)_{0.5}(Nb,Ni,Va)_{0.5}$. Both models give rise to nearly identical agreements to the experimental data within experimental uncertainty. The symmetric model is preferable in thermodynamic calculations of multi-component systems.

(iii) The presented liquidus projection and reaction scheme establish the constitution of the Al–Nb–Ni system over wide temperature and composition ranges, which is of interest for engineering applications as well as basic materials research.

Acknowledgements

The financial support from the Accelerated Insertion of Materials Program of DARPA and USAF through the contract, F33615-00-C-5215, is greatly acknowledged. Thanks are also due to Dr. Dan Backman of GE for his interest in this work. One of the authors (Yong Du) gratefully acknowledges the Furong Chair Professorship Program released by Hunan Province of the People's Republic of China for financial support.

References

[1] Sauthof G. Trans Nonferrous Met Soc China 1999;326 (Special issue): 326.

[2] Chen W, Yang W, Chang KM, Mannan SK, deBarbadillo JJ. In: Chang KM, Srivastava SK, Furrer DU, Bain KR, editors. Advanced Technologies for Superalloy Affordability. Tennessee, USA: TMS; 2000. p. 93.

[3] Kumar KS. Inter Mater Rev 1990;35(6):293.
[4] Wood JE, Goldman E. In: Sims CT, Stoloff NS, Hagel WC, editors. Superalloys II. New York, USA: John Wiley and Sons; 1987. p. 359.
[5] Schubert K, Meissner HG, Raman A, Rossteutscher W. Naturwiss 1964;51:287.
[6] Raman A, Schubert K. Z Metallkd 1965;56(2):99.
[7] Benjamin JS, Giessen BC, Grant NJ. Trans Metall Soc AIME 1966;236:224.
[8] Markiv VY, Matushevskaya NF, Kuz′ma YB. Russ Metall 1966; 6:72.
[9] Shoemaker CB, Shoemaker DP. Acta Crystallogr 1967;23:231.
[10] Mints RS, Belyaeva GF, Malkov YS. Russ J Inorg Chem 1962; 7:1236.
[11] Arbuzov MP, Chuprina VG. Izv Vysshikh Uchebn Zavedenii, Fiz 1963;5:82.
[12] Kornilov II, Mints RS, Guseva LN, Malkov YS. Russ Metall 1965;6:93.
[13] Hunt CR, Raman A. Z Metallkd 1968;59(9):701.
[14] Guseva LN, Mints RS, Malkov YS. Russ Metall 1969;5:120.
[15] Thompson ER, Lemkey FD. Trans Q Am Soc Met 1969; 62(1):140.
[16] Cisse J, Davies RG. Metall Trans 1970;1:2003.
[17] Duvall DS, Donachie MJ. J Inst Metals 1970;98:182.
[18] Lemkey FD, Thompson ER. In: Proc Conf on In Situ Composites Vol.II. National Academy of Science–National Academy of Engineering, Washington, 1973, p. 105.
[19] Smarov AK, Smagulov DU, Askarov MS. Metallurgiya Obogashch i Metalloved, Alma-Ata 1979:133.
[20] Nash P, Kavishe FPL, West DRF. Met Sci 1980;14(4):147.
[21] Ochiai S, Oya Y, Suzuki T. Bulletin of Research Laboratory of Precision Machinery and Electronics, Tokyo Institute of Technology 1983;51:1.
[22] Hong YM, Mishima Y, Suzuki T. In: High-temperature ordered intermetallic alloys 3. MRS Symp Proc 1989;133:429.
[23] Jia CC, Ishida K, Nishizawa T. Metall Mater Trans A 1994; 25(3):473.
[24] Ueyama T, Ghanem MM, Miura N, Takeyama M, Matsuo T. In: Chandra T, Sakai T, et al, editors. THERMEC ′97, Int Conf Thermomech Process Steels Other Mater. Warrendale, PA: 2nd. Minerals, Metals & Materials Society; 1997. p. 1753.
[25] Miura S, Hong YM, Suzuki T, Mishima Y. J Phase Equilib 2001; 22(3):345.
[26] Kaufman L, Nesor H. Metall Trans A 1975;6A:2115.
[27] Huang W, Chang YA. Intermetallics 1998;6:487.
[28] Huang W, Chang YA. Intermetallics 1999;7:625.
[29] Saunders N. System Al–Nb. In: Ansara I, Dinsdale AT, Rand MH, editors. COST 507-Thermochemical database for light metal alloys. European Commission EUR 18499 EN, Luxembourg, 1998, p. 69.
[30] Bolcavage A, Kattner UR. J Phase Equilibria 1996;17(2):92.
[31] Dupin N, Ansara I, Sundman B. CALPHAD 2001;25(2):279.
[32] Redlich O, Kister AT. Indust Eng Chem 1948;40:345.
[33] Dinsdale AT. CALPHAD 1991;15:317.
[34] Inden G. Proc Project Meeting, CALPHAD V, Max-Planck Institute for Metal Research, Dusseldorf, 1976, p. 1–13.
[35] Hillert M, Jarl M. CALPHAD 1978;2:227.
[36] Hillert M, Staffansson LI. Acta Chem Scand 1970;24:3618.
[37] Sundman B, Ågren J. J Phys Chem Solids 1981;42:297.
[38] Ansara I, Sundman B, Willemin P. Acta Metall 1988;36(4):977.
[39] Ansara I, Dupin N, Lukas HL, Sundman B. J Alloy Compounds 1997;247:20.
[40] Huang W, Chang YA. Intermetallics 1999;7:863.
[41] Pandat—Phase diagram calculation engine for multi-component systems, CompuTherm LLC, 437 S. Yellowstone Dr., Suite 217, Madison, WI 53706, USA, 2000.
[42] Sundman B, Jansson B, Andersson JO. CALPHAD 1985;9:153.
[43] Liu ZK, Chang YA. Metall Mater Trans A 1999;30:1081.
[44] Dupin N, Ansara I. Z Metallkd 1999;90:76.
[45] Du Y, Schmid-Fetzer R, Ohtani H. Z Metallkd 1997;88(7):545.